Geoderma 443 (2024) 116830

Contents lists available at ScienceDirect

Geoderma

journal homepage: www.elsevier.com/locate/geoderma

Soil colloids as binding agents in the formation of soil microaggregates in wet-dry cycles: A case study for arable Luvisols under different management

Ni Tang [a,b,*], Stefan Dultz [c], Daniel Gerth [a,b], Erwin Klumpp [a]

[a] Institute of Bio- and Geosciences, Agrosphere (IBG-3), Forschungszentrum Jülich GmbH, Wilhelm-Johnen-Straße, 52425 Jülich, Germany
[b] Institute for Environmental Research, Biology V, RWTH Aachen University, Worringerweg 1, D-52074 Aachen, Germany
[c] Institute of Soil Science, Leibniz Universität Hannover, Herrenhäuser Straße 2, 30419 Hannover, Germany

ARTICLE INFO

Keywords:
Soil microaggregation
Field flow fractionation
Size distribution of aggregates
Elemental composition

ABSTRACT

In the hierarchical model of soil aggregates, small soil microaggregates (small SMA; <20 μm) are often considered to be fundamental building units at the micron scale. Below which, soil colloids (<1 μm) have recently been proposed as binding agents of (micro)aggregates. However, the way in which soil colloids contribute to the formation and stability of soil micro- and macroaggregates remains largely unknown. For clarification, we evaluated potential impacts of the colloidal content, particularly the <450 nm colloids, on the aggregation of small SMA. Free water stable small SMA and <450 nm colloids were isolated from Ap-horizons of Stagnic Luvisols under different management (cropped and bare fallow). The size-resolved elemental composition of the <450 nm colloids was analyzed by asymmetric flow field-flow fractionation in combination with an inductively coupled plasma mass spectrometer and an organic carbon detector. To vary the colloidal content in small SMA, (1) suspensions containing different amounts of <450 nm colloids were added in small SMA, or (2) <1 μm colloids were removed from small SMA by centrifugation. In the maximum colloidal addition treatment, the mass ratios of added colloids to small SMA were 3.0 and 5.1 wt% for the cropped and bare fallow soil samples, respectively. Aggregation of small SMA with different colloidal amounts was performed in three successive wet-dry cycles. Afterwards, the size distribution of the resulting aggregates was measured by laser diffraction. Our results indicated that, in wet-dry cycles, colloids were important binding agents for the formation of SMA. Their presence, especially those <450 nm, was likely to support the formation of solid bridges during drying at particle contacts of 1–10 μm small SMA, favoring hereby SMA build-up in a relatively small size range of 1–40 μm. In contrast, the absence of <1 μm colloids in small SMA led to a preferential generation of relatively large aggregates in wet-dry cycles, i.e., typically with sizes >40 μm up to 1700 μm in maximum. Our study on aggregation in wet-dry cycles revealed that the colloidal content has a controlling effect on the size distribution of resulting aggregates by acting as a binding agent and provides hereby new insights into the evolvement of aggregate hierarchy in soils.

1. Introduction

As structural subunits of soils, aggregates are porous structures formed during pedogenesis, sustaining various soil functions such as organic matter and nutrient cycling, water retention, and gaseous exchange (Rabot et al., 2018; Totsche et al., 2018). Based on their sizes, soil aggregates are often grouped into soil macroaggregates > 250 μm and soil microaggregates <250 μm (SMA). Small SMA <20 μm are considered to be fundamental assembling blocks at the micron-scale of the highly hierarchical aggregate structure of soils (Totsche et al., 2018), thereby contributing to the development of their large-size counterparts. In turn, disintegration of large-size aggregates, e.g., macroaggregates, results in the release of SMA. These dynamic changes in aggregate structures are often mirrored in soil functions and processes. For example, in a recent modeling study, it has been demonstrated that the dynamic re-arrangement of SMA may affect the organic carbon turnover

* Corresponding author at: Institute of Bio- and Geosciences, Agrosphere (IBG-3), Forschungszentrum Jülich GmbH, Wilhelm-Johnen-Straße, 52425 Jülich, Germany.
E-mail address: n.tang@fz-juelich.de (N. Tang).

https://doi.org/10.1016/j.geoderma.2024.116830
Received 23 June 2023; Received in revised form 13 November 2023; Accepted 18 February 2024
Available online 21 February 2024

in soils (Zech et al., 2022). Similarly, aggregate dynamics can also influence the temporal distribution, mobility, and degradation of contaminants (Nam et al., 2003; Wang et al., 2018; Zhang and Liu, 2018). By implementing wet-dry cycles on soil aggregates, Hochman et al. (2021) found that changes in the aggregate structure, i.e., formation or disintegration, can either suppress or promote the leaching of pesticides, impacting their fate in soils. Hence, insights into aggregate development and dynamics may also advance our understanding of these soil functions and processes, respectively.

Binding agents, varying with aggregation at different hierarchical levels, have been suggested to be crucial to both aggregate formation and stability. For a bottom-up formation pathway, macroaggregates could be built up from SMA and stabilized by temporary binding agents such as roots and hyphae via enmeshment and compaction, as well as other less decomposed plant-derived organic matter (Blanco-Canqui and Lal, 2004; Oades and Waters, 1991; Six et al., 2000; Totsche et al., 2018). Macroaggregates are prone to disintegration under mechanical and hydraulic forces (e.g., tillage and slaking) (Six et al., 2000), whereas the structural integrity of SMA usually remains under the same external stress. Accordingly, binding agents of SMA are presumably different from those of macroaggregates (Oades and Waters, 1991; Totsche et al., 2018). It has been suggested that microbial-derived and -processed OM, in particular, favor the formation of SMA by their gluing nature (Lehmann et al., 2007; Verchot et al., 2011), while small-sized inorganic constituents such as clay minerals, metal (hydr)oxides and carbonates could act as cementing agents contributing to the formation of SMA and their composite buildings units (Krause et al., 2020; Totsche et al., 2018). The tendency of these components to enrich in small size fractions in soils (Kleber et al., 2015) likely endows colloids (<1 μm) and their nanoparticulate sub-fraction (<100 nm) with gluing and/or cementing features, making them potential binding agents for SMA formation (Asano and Wagai, 2014; Krause et al., 2020; Totsche et al., 2018). In addition, interactions between submicron-sized minerals and OM could initiate the formation of small SMA or colloidal organo-mineral/metal associations (Totsche et al., 2018). The latter has been assumed to function as effective or persistent binding agents, promoting the formation of larger SMA with clay minerals and primary particles (Asano et al., 2018; Wagai et al., 2020).

Apart from the composition, chemical and physical properties (i.e., surface charge, size, and shape) of colloids could also support the binding agent role, especially under wet-dry cycles, a common process that most temperate soils undergo due to the variation in soil moisture (Totsche et al., 2018). Theoretically, when soils are subjected to drying, capillary forces created by water menisci bring the otherwise dispersed colloidal or clay-sized aggregate forming materials into contact, strengthening near field interactions (Guhra et al., 2022; Totsche et al., 2018). Further, capillary forces between large particles tend to arrange and concentrate small size particles, such as colloids or clay particles, at contact areas of large particles (Guhra et al., 2022; Horn and Dexter, 1989; Horn et al., 1994). As a result, large particles are bridged by small particles promoting the formation and stability of aggregates. This mechanism was recently verified in model systems of silica spheres, illite, and kaolinite with diameters <100 μm by Seiphoori et al. (2020), emphasizing the stabilizing effect of micron- and submicron-sized on large sized particles (e.g., 5–100 μm) into stable aggregates by forming solid bridges after drying. Based on these findings, the authors proposed that stability of unconsolidated soils may be enhanced by addition of nanoparticles. In a following work to testify this postulation, Seiphoori and Zamanian (2022) could show that grouting the <0.25 μm montmorillonite particles into the predominantly silt-sized sediment loess greatly reduced its collapse potential after drying of the grout. While findings with model components are enlightening, contributions of soil colloids to the evolvement and stabilization of aggregates in soils remain less clear. One reason is that, besides pure mineral and organic soil components, soil colloids can also occur in forms of organo-mineral and/or mineral–mineral associations (Jiang et al., 2015; Totsche et al., 2018), potentially rendering together with the complexity of soil matrix a different behavior in aggregate formation processes. Another obstacle is that, due to the overlap of their sizes, in many studies solid colloids were not well distinguished from dissolved phases (e.g., dissolved organic matter and salts), which are operationally defined as fractions passing through the <450 or <220 nm filters. Accordingly, the role of soil colloids, particularly those with sizes <450 nm, in soil aggregation might be overlooked or tangled with that of the truly dissolved phase. With the advent of the asymmetrical flow field flow fractionation (AF4) technique, colloidal particles between 0.7 − 450 nm can be separated from the dissolved phase and the elemental compositions of their size fractions can be determined.

The quantity and quality of gluing and cementing agents in soils can vary with land use, soil management, and soil type, and thus leading to different aggregate dynamics. For arable soils, agricultural practices are of great importance as they are frequently found to affect SOC/SOM qualitatively and quantitatively, thereby influencing the formation and stabilization of soil aggregates at different hierarchical levels (Blanco-Canqui and Lal, 2004). The lack of continuous OM input in silty loam soils under long-term bare fallow, for instance, tends to result in a progressive loss of macroaggregate structures (Paradelo et al., 2016). Meanwhile, in the soils of our study, loss of SOC in the <20 μm size fraction, which was already observed after a decade bare fallow (Meyer et al., 2017), along with changes in SOM quality (i.e., accumulation of older SOM, Siebers et al., 2024) in the <20 μm size fraction may influence the formation and stabilizing of larger microaggregates, as they comprised clay-sized organo-mineral associations and small SMA which are considered to be fundamental building units at the micron scale (Totsche et al., 2018).

In the current study, to investigate the impact of fine soil colloids on the aggregation of small SMA under wet-dry cycles, Ap horizons of Luvisols under cropped and 14 years of bare fallow (Jiang et al., 2015; Meyer et al., 2017) were studied. Colloids <450 nm and water stable small SMA were separated from fine soil samples. We hypothesized that i) the high abundances of soil colloids promote the aggregation of small SMA in wet-dry cycles by acting as binding agents, and ii) due to the loss of OC in small SMA, the size of aggregates formed in wet-dry cycles are smaller in the bare fallow soils.

2. Materials and methods

2.1. Soil sampling and fractionation

The sampling site is located at Selhausen (50°52′08″ N, 6°26′59′ E), which belongs to the German Lower Rhine Embayment, with a mean annual temperature of 10.3 °C and precipitation of 854 mm. Two parallel fields under different management conditions are situated at this site within a distance of 100 m. The parent materials of soil formation are loess together with alluvial loam and gravel. One field has been converted into bare fallow management since 2005 with regular herbicide application (Meyer et al., 2017; Schweizer et al., 2024; denoted as “bare fallow” field hereafter). Additionally, mechanical tillage (a 5 cm deep ploughing) was practiced once per year between 2005 and 2010. The parallel cultivated field in the immediate vicinity was marked as the cropped field, which has been continuously cultivated mainly with sugar beet and winter wheat for a century. In November 2019, the Ap horizon (5–25 cm) of these soils were collected in triplicate from the west downslope plots of the cropped and bare fallow fields. After sampling, the field-fresh soil samples were sealed in plastic bags and stored in a cool chamber at 4 °C. The soils are classified as Stagnic Luvisol (IUSS Working Group WRB, 2007) with a silt loam texture (Table 1). However, Stagnic properties are relatively weak and could not be observed in the Ap horizon. Soil properties of the cropped and bare fallow soils including pH values and elemental concentrations are given in Table 1.

The isolation of free water stable small SMA (<20 μm) was performed using wet-sieving according to Krause et al. (2018) (Fig. 1). In

Table 1
Soil texture and properties of bulk soils from cropped and bare fallow sites.

	Texture (%)			pH	Elemental concentration (mg g^{-1})					
	Sand	silt	clay	$CaCl_2$ extracted	C	N	[a]Fe (DCB)	Fe (Oxlate)	Al (DCB)	Al (Oxlate)
Cropped	15.6	58.0	26.3	6.9 ± 0.2	10.0 ± 0.6	1.3 ± 0.1	6.3	2.5	1.0	0.9
Bare fallow	14.8	56.8	28.3	6.3 ± 0.2	10.1 ± 1.7	1.3 ± 0.1	6.2	2.8	1.0	0.9

[a] The average oxalate and dithionite-citrate-bicarbonate (DCB) extractable Fe and Al were adopt from (Siebers et al., 2024) and (Jiang et al., 2015), respectively.

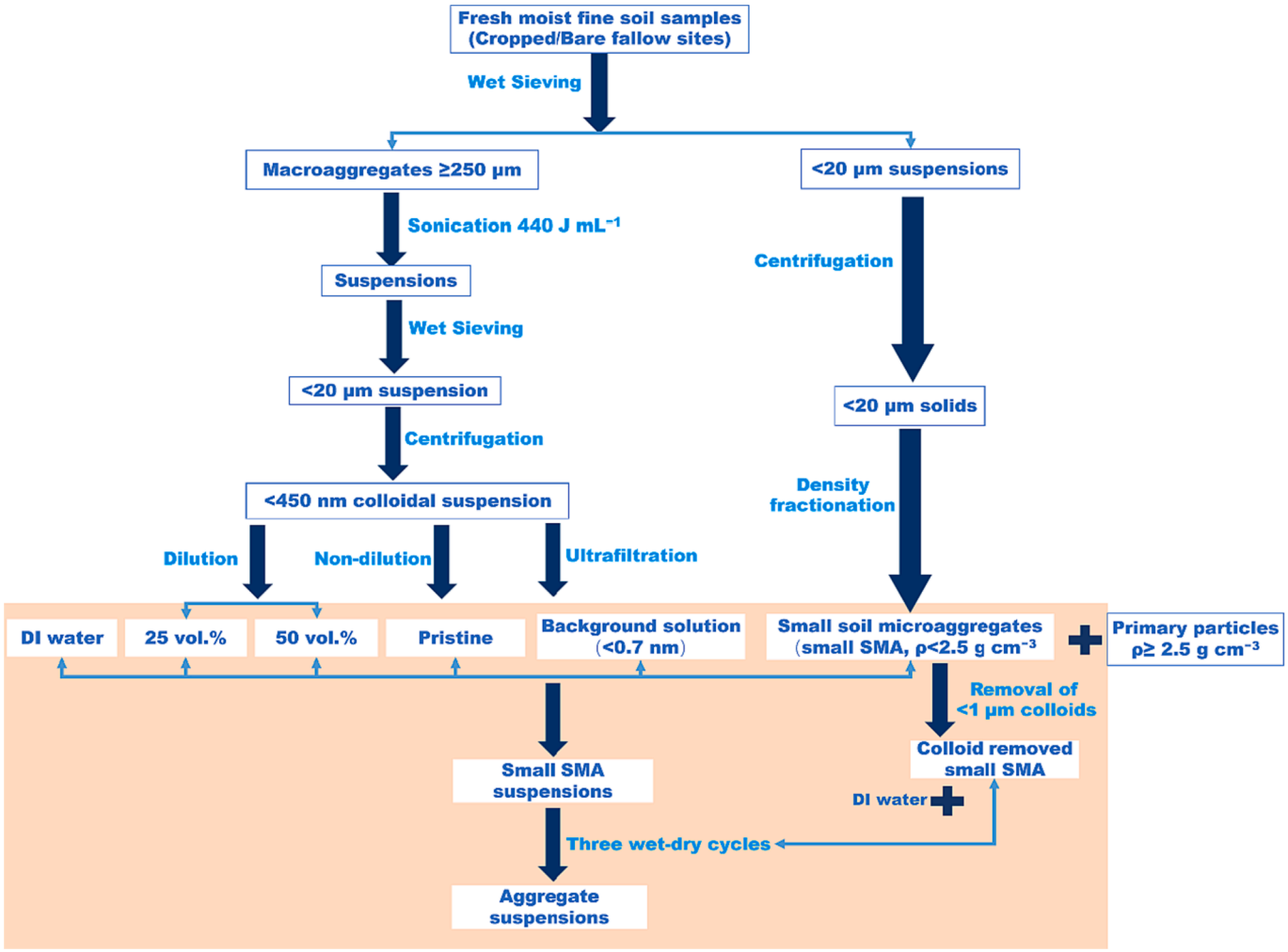

Fig. 1. Scheme illustrating the procedure of soil size fractionation and aggregation in wet-dry cycles. Among different treatments, small soil microaggregates (SMA) were suspended in deionized (DI) water, diluted <450 nm colloidal suspensions (25 and 50 vol%), pristine colloidal suspensions (non-diluted), and background (BG) solutions, respectively. In treatments with colloid removal, small SMA with reduced shares of <1 μm colloids were suspended in deionized water.

short, 60 g of field-moist samples were pre-wetted in deionized water for 5 min on a sieve tower consisting of 4 sieves with a mesh size of 2000, 250, 53, and 20 μm, respectively. The sample was then wet sieved under constant shaking (30 rotation per minute; RPM) for 10 min. Macroaggregates that remained on the 250 μm sieve were collected for the sequentially colloidal separation, which was performed according to the description in the section 2.2. The 11 L suspension containing <20 μm fraction was centrifuged at 5346 × *g* for 8 min (Heraeus MULTIFUGE 4KR, Thermo Scientific, Massachusetts, USA) to recover the solid phase.

According to Virto et al. (2008), density fractionation was performed using a sodium *meta*-tungstate (SMT; $Na_6O_{39}W_{12}{\cdot}H_2O$, Thermo Fisher Scientific, Massachusetts, United States) solution at $\rho = 2.5$ g cm^{-3} to separate small SMA (ρ <2.5 g cm^{-3}) from primary particles (ρ > 2.5 g cm^{-3}). Afterwards, the obtained small SMA were washed using deionized H_2O until the electrical conductivity of the suspension reached ~ 5 μS cm^{-1}. The elemental concentrations of Si, Al, and Fe in small SMA were determined by inductively coupled plasma optical emission spectroscopy (ICP-OES; iCAP 7600, Thermo Fisher Scientific, Massachusetts, United States) while the total C and N contents were measured by elemental analysis (Vario MICRO cube, Elementar Analysesysteme GmbH, Langenselbold, Germany). Prior to the ICP-OES measurement, approximately 50 mg of small SMA samples were digested with 0.25 g of $Li_2B_4O_7$ at 1050 °C in a muffle furnace for 30 min. After digestion, the mixture was dissolved in 30 mL of 5 % HCl and diluted for the subsequent measurement.

2.2. Preparation of soil colloids suspensions

To vary the colloidal content in small SMA, colloids were added as a suspension (Fig. 1). For this purpose, soil colloids <450 nm were released from macroaggregates (250–2000 μm) of the cropped and bare fallowed fine soil samples that were separated by wet sieving (as described in the section 2.1). Macroaggregates were suspended in deionized water and subjected to an ultrasonic treatment (Digital Sonifier 450, Branson Ultrasonics corp., Connecticut, USA) with an energy of 440 J mL^{-1} and sequentially wet-sieved with the sieving tower. The obtained <20 μm suspension was centrifuged at 9800 × *g* for 13 min (Avanti JXN-30, Beckman Coulter, California, USA), which was calculated based on the Stockes' law. Thereafter, the <450 nm colloidal suspension was collected from the supernatant. The cutoff of the isolated colloids was verified by dynamic light scattering (DLS, Nano-zs, Malvern Panalytical, Malvern, UK, **Supporting information, SI, Figure S1**), and pH values of their suspensions were 7.63 ± 0.10 and 7.10 ± 0.20 for the cropped and bare fallow soils, respectively.

To prepare colloidal suspensions in different concentrations, the obtained <450 nm colloidal suspension was diluted with deionized water. Specifically, 25 and 50 %v/v colloidal suspensions were obtained by addition of 45 and 30 mL of deionized water into glass bottles (100 mL; Duran®) containing 15 and 30 mL of the pristine <450 nm colloidal suspensions, respectively. In addition, background solutions, containing partially the <0.7 nm fraction (<1 kDa, ~0.7 nm) of pristine <450 nm colloidal suspensions (non-diluted), were separated with tangential flow filtration (1 kDa, Minimate TFF, Pall, USA). The concentrations of OC, Si, Al, Fe, Ca, Mg, and P in background solutions were given in Table 2.

2.3. Wet-dry cycles

Before wet-dry cycles (Fig. 1), subsamples of small SMA from the cropped and bare fallow soil samples with a dry mass of ~ 0.75 g were suspended in 30 mL of colloidal suspensions (pristine, 25 and 50 vol% diluted, respectively), background solutions, and deionized water, respectively. The 30 mL of <450 nm pristine colloidal suspensions contained on average 21.6 and 38.6 mg dry colloids for the cropped and bare fallow soil samples, respectively. In comparison to these treatments, subsamples of small SMA were repeatedly centrifuged and decanted to decrease the content of the colloidal fraction (<1 μm). Afterwards, small SMA were suspended in deionized water and denoted as the colloidal removal treatment. The size distribution of small SMA in different treatments was immediately measured by laser diffraction (LA-950, Horiba, Kyōto, Japan).

The wet-dry cycles were carried out on 10 mL of small SMA suspensions at room temperature in glass Petri dishes according to the procedure described in Krause et al. (2020). Shortly, small SMA suspensions were subjected into 3 wet-dry cycles, and each of them consisted of a 10 h wetting period, which is followed by a 14 h drying period at room temperature. Complete air drying of the samples was monitored via weight loss. After that, the corresponding evaporated volume was replaced by deionized water with a pipette to allow the particles to re-suspend for the wetting phase. The process well corresponded to the fast-wetting, where samples undergo a rapid immersion and transition from a well-aerated state into a water-suspended state (Kaiser et al., 2015; Le Bissonnais, 1996). After three completed wet-dry cycles, the resulting aggregates were re-suspended in deionized water, and their size distributions were immediately determined by laser diffraction in suspension form. An aliquot of aggregate suspensions was passed through a 0.45 μm filter (P667.1, Rotilabo, Carl Roth GmbH & Co. KG, Karlsruhe, Germany), and the filtrate was stored at 4 °*C* for further analysis.

2.4. Particle size distribution

The volume-based particle size distributions of SMA before and after wet-dry cycles were determined using laser diffraction, which is capable of measuring size distribution of a wide size range of particles from ~ 10 nm to 3000 μm. Under continuous stirring, the suspended samples were measured in a flow-through cell where light in two wavelengths was applied (650 and 405 nm). The data about scattering angle and light intensity were measured by the detectors and transformed by a software algorithm into a volume-based size distribution using the Mie theory provided by the manufacturers' software (Amelung et al., 2024; Beganowski et al., 2018; Krause et al., 2020).

2.5. Asymmetric field flow fractionation

The size-resolved concentrations of OC, Si, Al, Fe, Ca, Mg, and P in colloids (0.7–450 nm) before and after three wet-dry cycles were measured by asymmetric flow field-flow fractionation (AF4, Postnova Analytics, Landsberg am Lech, Germany) coupled with an organic carbon detector (OCD; DOC laboratory Dr. Huber, Karlsruhe, Germany) and an inductively coupled plasma mass spectrometer (ICP-MS; Agilent 7500, Agilent Technologies, California, USA). Elemental quantification was performed by a post channel calibration approach (Nischwitz et al., 2016). The AF4 separation channel was equipped with a 500 μm spacer and a 1 kDa PES membrane. During the measurement, a 25 μM NaCl solution was used as the carrier solution. The 0.5 mL of sample was injected into the channel at a flow rate of 0.3 mL min^{-1}. The sample was

Table 2
Concentrations of C, N, Fe, Al, and Si (mg g^{-1}) in the small SMA along with elemental concentrations (μmol L^{-1}) of organic carbon (OC), Mg, Al, Si, P, Ca, and Fe in the <0.7 nm fraction of the pristine (non-diluted) and diluted (25 and 50 vol%) <450 nm colloidal suspensions and background (BG) solutions from the cropped and bare fallow soils. Means (n = 3) marked with different lowercase letters indicate significant differences between different soils.

	Elemental concentrations in small SMA (mg g^{-1} SMA)				
	C	**N**	**Fe**	**Al**	**Si**
Cropped	22.8 ± 1.3a	3.4 ± 0.3a	35.9 ± 2.3a	64.0 ± 4.0a	311.3 ± 20.0a
Bare fallow	14.6 ± 4.0b	2.3 ± 0.4b	18.9 ± 0.7b	36.8 ± 1.2b	211.0 ± 6.6b

	Elemental concentrations in the <0.7 nm fraction (μmol L^{-1})						
	OC	**Mg**	**Al**	**Si**	**P**	**Ca**	**Fe**
Cropped							
25 vol%	21.9 ± 21.4	7.9 ± 0.3	44.3 ± 3.0	169.0 ± 12.6	4.0 ± 0.5	3.0 ± 0.8	26.6 ± 1.2
50 vol%	103.9 ± 89.6	10.6 ± 3.6	52.2 ± 30.6	251.1 ± 53.1	8.7 ± 1.4	6.1 ± 0.9	43.0 ± 9.6
Pristine	410.7 ± 214.2	30.6 ± 15.3	180.3 ± 142.5	547.3 ± 232.0	18.9 ± 3.9	13.5 ± 12.0	55.0 ± 32.1
BG solution	113.1 ± 9.5	2.2 ± 1.3	0.5 ± 0.2	95.2 ± 6.1	1.8 ± 0.2	12.9 ± 7.1	0.1 ± 0.1
Bare fallow							
25 vol%	92.8 ± 44.7	12.0 ± 1.9	55.0 ± 16.4	213.2 ± 36.9	10.9 ± 3.2	3.6 ± 1.6	19.2 ± 7.1
50 vol%	120.0 ± 114.5	17.6 ± 9.2	76.7 ± 52.4	345.5 ± 103.5	21.7 ± 4.4	8.2 ± 4.3	21.8 ± 17.1
Pristine	472.8 ± 243.2	43.1 ± 6.9	266.5 ± 142.7	827.0 ± 160.6	48.1 ± 10.6	21.3 ± 15.8	39.6 ± 26.4
BG solution	102.9 ± 22.5	4.3 ± 1.3	0.2 ± 0.0	94.2 ± 2.4	6.4 ± 2.4	9.9 ± 2.5	0.1 ± 0.0

then focused in the channel for 12 min using a focus flow of 3.2 mL min^{-1} and a cross flow of 3 mL min^{-1}. After a 1 min transition, the focus flow was switched off, and the crossflow rate was kept constant for 5 min. The crossflow subsequently reduced exponentially from 3 to 0 mL min^{-1} in 55 min with the power mode and remained at 0 mL min^{-1} for another 50 min. The elution of spherical latex standards with sizes of 20, 60, 100, 220, and 600 nm was carried out under the same AF4 separation condition as soil colloidal samples (**Figure S2**). However, given the heterogeneity of natural colloids, size cutoffs at 55 and 270 nm of size fractions were obtained from online AF4-DLS measurements (Missong et al., 2018; Tang et al., 2022) (**Figure S3**). The total elemental concentrations (Fe, Al, Si, Ca, and Mg and OC) of <450 nm colloidal suspensions, comprising those of the <0.7 and 0.7–450 nm fractions, were determined by AF4 system without fractionation (crossflow at 0 mL min^{-1}). The elemental concentrations in the <0.7 nm fraction were acquired by subtracting those in the 0.7–450 nm fraction from the total elemental concentrations.

2.6. Statistical analyses

All statistical analysis was conducted in Origin (OriginPro 2022, Originlab, Massachusetts, USA). The Shapiro-Wilk test was used for testing the normality of data distribution. Differences in the percentage of aggregates in different size ranges between the bare fallow and cropped soils among treatments were evaluated by performing two-way ANOVA with a Bonferroni post hoc test at a significant level of $\alpha = 0.05$. Instead, one-way ANOVA was preformed to evaluate differences in elemental concentrations of the small SMA between the bare fallow and cropped samples. Impacts of the abundance of the <450 nm and <1 μm colloids in suspensions of small SMA on the size distribution of

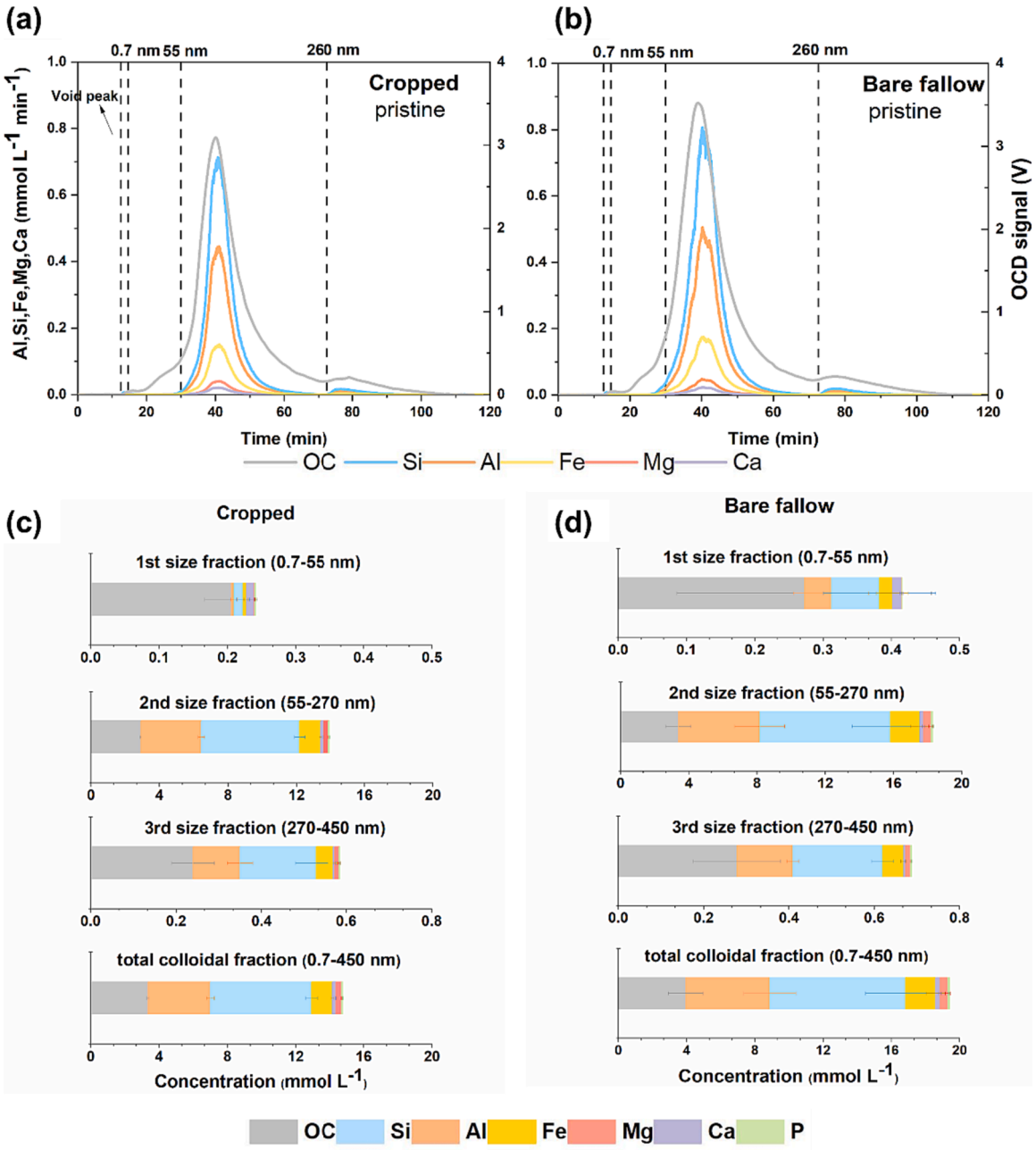

Fig. 2. Fractograms of the pristine 0.7–450 nm colloids (non-diluted) from the cropped (**a**) and bare fallow (**b**) soils, and elemental concentrations in different size fractions (**c** and **d**) of these colloids. These 0.7–450 nm colloids were released from macroaggregates > 250 μm of the cropped and bare fallow site by sonication at 440 J mL^{-1}.

aggregates after wet-dry cycles were evaluated by Pearson correlation. In addition, Pearson correlation was also conducted among the elemental concentrations (Fe, Al, Si, Ca, Mg, and OC) in the added <450 nm fraction, including the <0.7 and 0.7–450 nm fractions, and the △P40. The △P40 represented, after wet-dry cycles, in relative to the deionized water treatment, the increased percentage of the 1–40 μm aggregates in other treatments, where small SMA were treated with colloidal suspensions (pristine colloidal suspension, 50 vol% colloidal suspension, and 25 vol% colloidal suspension) and background solutions.

3. Results

3.1. Elemental concentration of the free water stable small microaggregates and the 0.7–450 nm soil colloids

Unlike the fine earth <2 mm, where the total C and N contents were comparable for the cropped and bare fallow samples, the total C and N contents in the small SMA from the cropped soil were significantly higher than those from the bare fallow soil (Table 2). A similar trend was also found for the Fe, Al, and Si concentrations of the small SMA from these two sites.

For both the added 0.7–450 nm colloids (Fig. 2**c and 2d**) and the 0.7–450 nm colloids originally existing in the small SMA (**Figure S4**), concentrations of Si, Al, OC, Fe, Ca, Mg and P between bare fallow and cropped soil samples were not significantly different ($P > 0.05$), although those of the bare fallow ones were slightly higher. Moreover, three subsize fractions were identified by AF4 for these 0.7–450 nm colloids (Fig. 2**a and 2b; Figure S4**), containing the first (0.7–55 nm), second (55–270 nm), and third (270–450 nm) size fractions. Regarding the added 0.7–450 nm colloids, for both the cropped and bare fallow soil samples, fractograms were predominant by the second size fraction (55–270 nm), where 87–97% of the 0.7–450 nm colloidal OC, Si, Al, Fe, Mg, and Ca were present (Fig. 2). As for the elemental composition, the first size fraction featured with a relatively high abundance of OC along with the presence of Si, Al, Ca, Fe, and Mg (Fig. 2**c and 2d**), whereas comparable compositions were found for the second and third size fractions (Fig. 2**c and 2d**), comprising high abundances of Si, Al, OC, and Fe. Moreover, the distribution pattern of size fractions was not significantly changed when diluting these colloids with deionized water (**Figure S5**).

Similar to the added 0.7–450 nm colloids, AF4 measurements on subsamples of the 0.7–450 nm colloids originally existing in the small SMA showed that, for both the bare fallow and cropped samples (**Figure S4**), the first size fraction (0.7–55 nm) was mainly composed of OC, while the second (55–270 nm) and third size fractions (270–450 nm) primarily comprised Si, Al, OC, and Fe. However, compared to the added 0.7–450 nm colloids, a higher proportion of the third size fraction was found for the 0.7–450 nm colloids originally existing in the small SMA (**Figure S4**), comprising 33–42 and 51–53% of the measured colloidal Si, Al, Fe, and OC for the cropped and bare fallow soil samples, respectively.

After wet-dry cycles, laser diffraction measurements indicated an extremely low abundance of the <1 μm colloids (Fig. 3 **and** **Table S1**, <~ 0.2 vol%). Also, AF4-ICP-MS/-OCD measurements clearly showed the presence of the 0.7–450 nm colloidal Si, Al, OC, Fe, and Mg but in relatively low concentrations (**Figure S7 and S8**). Furthermore, the pattern of fractograms was comparable among treatments (**Figure S7**); while most colloidal Si, Al, and Fe were present in the second size fraction, a large proportion of the 0.7–450 nm colloidal OC was found in the first size fraction (**Figure S7 and S8**).

3.2. Size distribution of the soil microaggregates

Before wet-dry cycles, for both the cropped and bare fallow soils, the volume-based size distributions were comparable in treatments where small SMA were suspended in colloidal suspensions, background solutions, and deionized water, respectively (Fig. 3**a** − **j**). They exhibited a bimodal pattern, peaking at around 0.3 and 6.7 μm, respectively (Fig. 3**a** − **j**). In these treatments, for the cropped and bare fallow soils, on average 93.7 and 89.4% of the detected particles were found in the size range of 1–20 μm, respectively, whereas the percentage of colloids between 0.1–1 μm varied among treatments representing 5.4–6.7% and 8.2–9.9% of the detected particles for the cropped and bare fallow soils, respectively (**Table S1**). Only ~ 0.6–2.2% of particles exceeded the size range of small SMA occurring in the size range of 20–40 μm (**Table S1**). In contrast, in the <1 μm colloid removal treatments, a unimodal distribution peaking at ~ 6.0 μm was observed (Fig. 3**k and 3 l**), with most of the particles (98.9 ± 0.4 and 95.7 ± 2.7% for the cropped and bare fallow soils, respectively) being present in the range of 1–20 μm (**Table S1**).

After wet-dry cycles, for both the cropped and bare fallow soils, the formation of large-size aggregates was observed, concomitant with the disappearance of the <1 μm colloidal particles (<0.2%, **Table S1**) and decreased abundances of 1–10 μm small SMA (Fig. 3). However, the size distribution pattern of the resulting aggregates varied among treatments. In the <1 μm colloid removal treatment, 83.4 ± 2.6 and 76.7 ± 6.5% of the detected particles were >40 μm with a maximum of ~ 1700 μm for the cropped and bare-fallow soils, and the rest of the particles were present in the range of 1–40 μm (**Table S1**). As a result, a bimodal size distribution pattern with peak values at 8.8 and 344 μm was observed for these treatments (Fig. 3**k and 3 l**). The deionized water (Fig. 3**a and 3b**) and background solution (Fig. 3**i and 3j**) treatments also showed a bimodal size distribution peaking at ~ 15 and 115 μm, with the 1–40 μm particles accounting for 51–77% of the detected particles (**Table S1**). In contrast, the abundances of the 1–40 μm SMA in the pristine colloidal suspension treatments were 80.7 ± 7.0 and 88.6 ± 4.9% for the cropped and bare fallow soils, respectively. This led to a unimodal-like size distribution pattern in these treatments with a peak at 13.2 μm (Fig. 3**g and 3 h**).

A significantly positive correlation was found between the volume-based abundance of the 1–40 μm SMA after wet-dry cycles and that of the <450 nm colloids (Fig. 4**a**) in small SMA suspensions before wet-dry cycles. A similar correlation was also found for the <1 μm colloids in small SMA suspensions and the 1–40 μm SMA after wet-dry cycles (Fig. 4**b**). The influence of elemental concentrations of the added 0.7–450 nm colloids on the size distribution of aggregates resulting from wet-dry cycles was evaluated by Pearson correlation as well, suggesting that the increased percentages of the 1–40 μm fraction (△P40) in other treatments relative to the deionized water treatments were positively correlated with the concentrations of the added 0.7–450 nm colloidal Ca, OC, Si, Al, Mg, and Fe (Table 3). In addition, the △P40 was also positively correlated with the concentrations of Mg, OC, Si, and Al ($p < 0.05$) in the <0.7 nm fraction, being more significantly with that of Ca in this fraction ($P < 0.01$).

4. Discussion

4.1. Composition of the 0.7–450 nm colloids participating in aggregation

Among treatments, the 0.7–450 nm colloids in small SMA suspensions were composed either or both of the added 0.7–450 nm colloids (Fig. 2 **and** **Figure S5**) and those originally existing in the small SMA (**Figure S4**). Three sub-sized fractions (0.7–55 nm, 55–270 nm, and 270–450 nm) were identified in these 0.7–450 nm colloids by applying AF4, in line with previous AF4 studies on other natural colloids from forest and arable soils (Li et al., 2021; Missong et al., 2018; Tang et al., 2022; Zhang et al., 2021). Moreover, the dominance of OC in the first size fraction (0.7–55 nm) of these colloids corroborated the findings on the nanoparticulate fraction of other arable Luvisols (Tang et al., 2022). The Fe and Al in this size fraction might occur as Fe and Al (hydr)oxides (Jiang et al., 2015), being capable of forming associations with OC

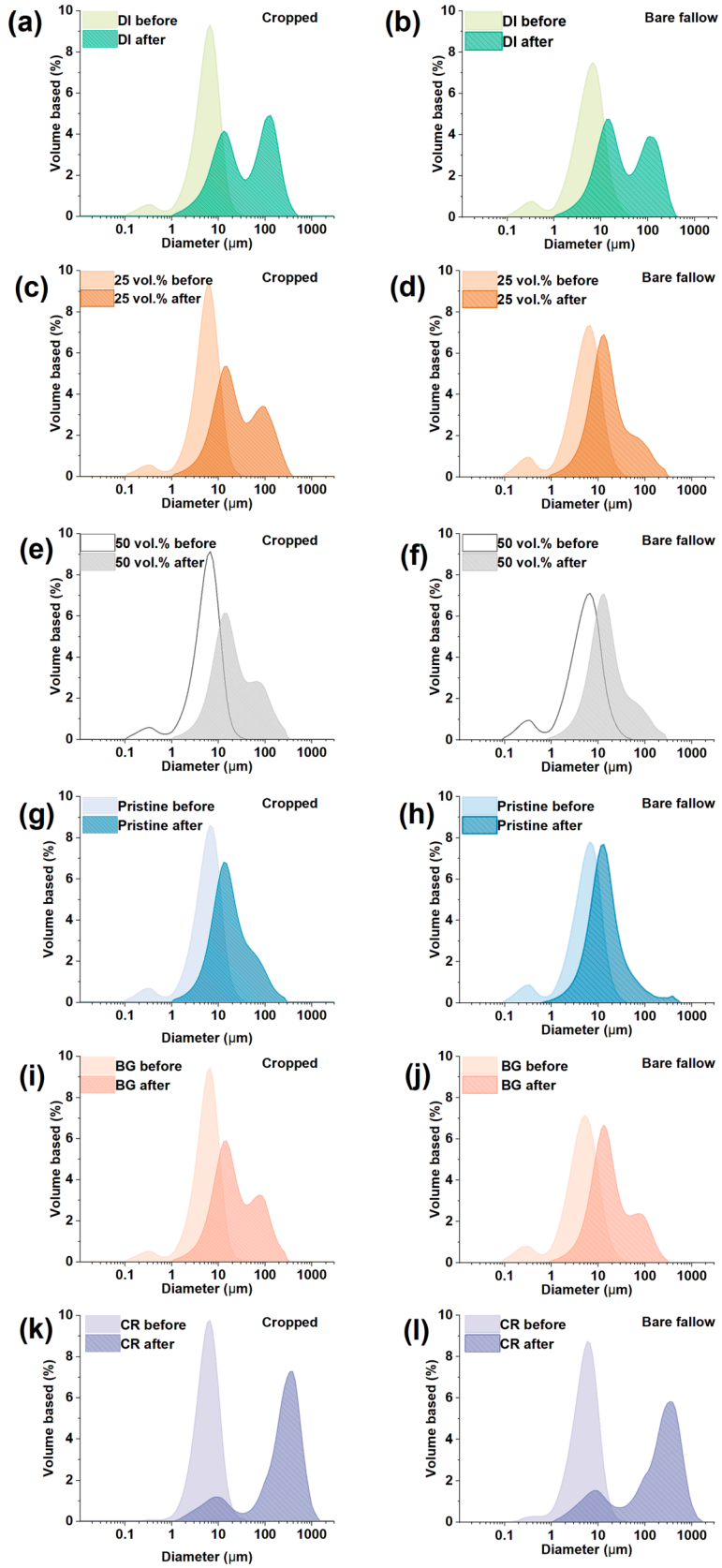

Fig. 3. Volume-based size distributions of small soil microaggregates (SMA) from the cropped and bare fallow soil samples among different treatments. The size distributions of aggregates were measured by laser diffraction in suspension before and after three wet-dry cycles. Among different treatments, small SMA were suspended in deionized water (DI, **a** and **b**), diluted colloidal suspensions (25 vol%, **c** and **d**; 50 vol%, **e** and **f**), pristine colloidal suspensions (non-diluted, **g** and **h**), and background solutions (BG, **i** and **j**), respectively. The CR refers to the colloidal removal treatments (**k** and **l**), where small SMAs with a reduction of the <1 μm colloids were suspended in deionized water.

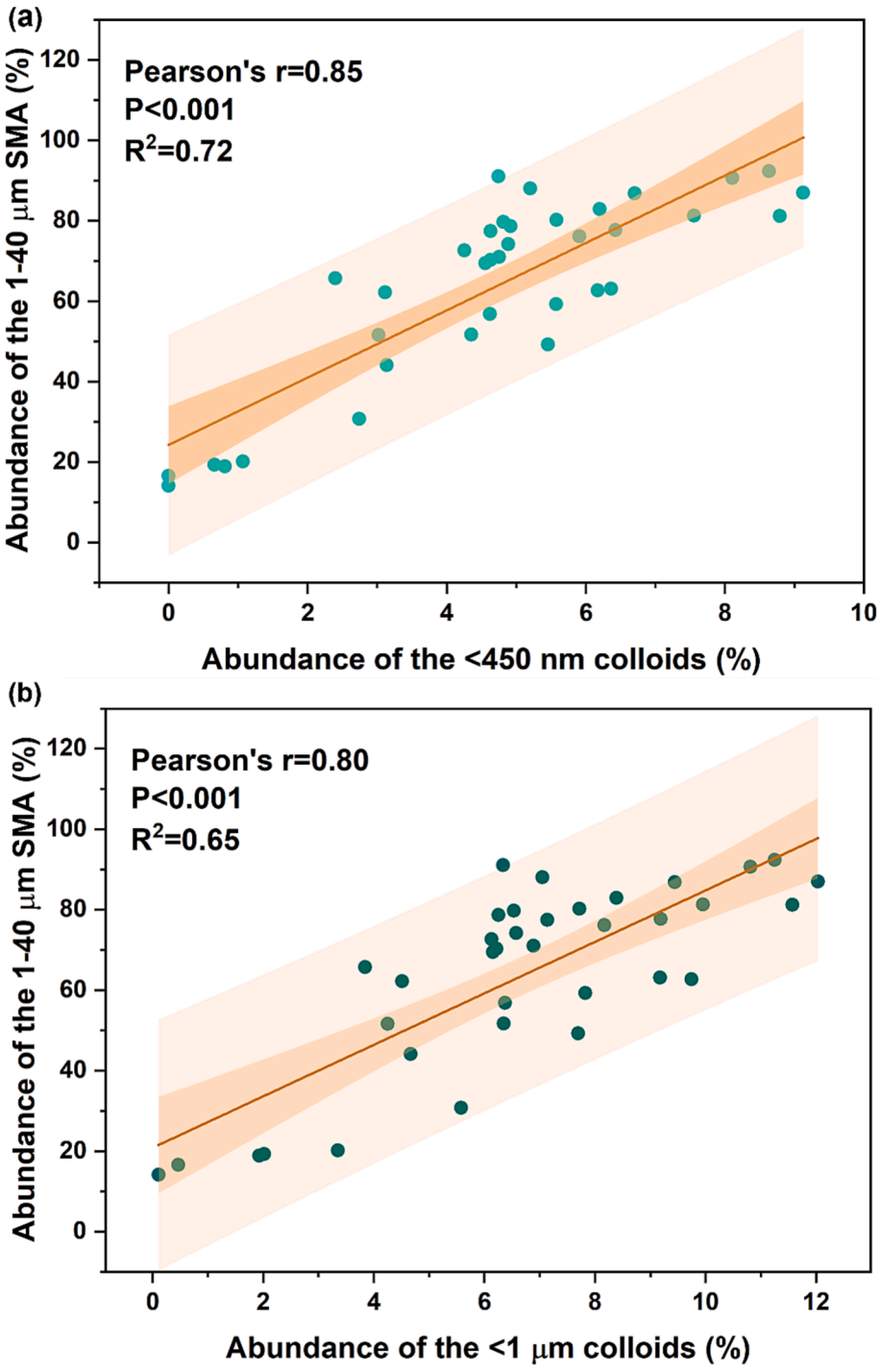

Fig. 4. Pearson correlation between the abundance of the <450 nm (a) and <1 μm colloids (b) in suspensions of small SMA before wet-dry cycles and the abundance of the 1–40 μm aggregates after wet-dry cycles (n = 36).

(Kleber et al., 2015; Mikutta et al., 2009). The existence of Fe (hydr) oxides and a small amount of Al (hydr)oxides in the <20 nm fraction of WDCs <225 nm from the same sampling sites was reported by Jiang et al. (2015), who peformed the oxalate and DCB extraction on WDCs and monitored their changes in Fe and Al concentrations before and after extractions by AF4 measurements. The Ca and Mg in this fraction could exist as cations and bridge negatively charged soil organic matter to form complexes (Bai et al., 2020; Lützow et al., 2006; Rowley et al., 2018).

In contrast to the first size fraction, mineral constituents were prevailing in the second (55–270 nm) and third (270–450 nm) size fractions (Fig. 2; **Figure S4 and S5**), which presumably consist of clay minerals and Fe and Al (hydr)oxides. Yet, the high abundance of Al in these fractions more likely results from different clay minerals rather than Al (hydr)oxides, since Jiang et al. (2015) observed that most of Al in WDCs <225 nm cannot be removed by DCB extraction. Clay mineralogy of the studied sites is characterized with a high abundance of illite along with the presence of kaolinite, vermiculite, smectite and quartz (**Figure S6**). Note, abundances of clay minerals in these colloidal size fractions might differ from those in the coarse clay fraction (<2 μm), i.e., by a higher share of smectite (Gonzalez and Laird, 2003; Laird et al., 2001). Mineralogy analysis on clay subfractions revealed that quartz, illite, and

Table 3
Pearson correlation between the △P40 and Fe, Al, Si, Ca, Mg, and OC concentrations in the 0.7–450 nm colloidal and <0.7 nm fraction in colloidal suspensions (pristine, 25 and 50 vol%) and background solutions that were added into small SMA. The 25 and 50 vol% colloidal suspensions were obtained from diluting the pristine colloidal suspension with deionized water.

	Elements						
	Ca	Mg	OC	Al	Si	P	Fe
	0.7–450 nm fraction						
△P40[a]	0.55**	0.53**	0.54**	0.54**	0.53**	0.54**	0.54**
	<0.7 nm fraction						
△P40	0.69**	0.53*	0.51*	0.50*	0.51*	0.48	0.38

[a] △P40 = $P40_i - P40_0$, $P40_0$: After wet-dry cycles, the percentage of the 1–40 μm aggregates in deionized water treatments, $P40_i$: After wet-dry cycles, the percentages of the 1–40 μm aggregates in colloidal suspension and background solution treatments. * and ** indicated $p < 0.05$ and < 0.01, respectively.

kaolinite were relatively enriched in the coarse clay fraction (0.2–2.0 μm) while smectite was the dominant mineral phase in the finer clay fraction (<0.2 μm) (Gonzalez and Laird, 2003; Laird et al., 2001). In addition to these clay minerals, average Si/Al molar ratios at ~ 1.6 in the 0.7–450 nm colloids and their subsize fractions for the cropped and bare fallow soil samples (Fig. 2**; Figure S4 and S5**) point to the potential existence of other Si-enriched components, such as quartz, alkali feldspar, and phytoliths (Nguyen et al., 2019). The overlap between OC and Si, Al, and Fe in AF4 fractograms (Fig. 2 **and Figure S5**) implies that OC was possibly associated with clay minerals, Fe (hydr)oxides, and their associations (Kleber et al., 2015). For the elements Ca and Mg detected in these fractions, it is likely that they are not only located in the structure of silicates, but, at circumneutral pH, have a marked share at the exchange sites and can contribute to the formation of clay mineral-OC associations by serving as cation bridges (Bronick and Lal, 2005; Lützow et al., 2006).

The observed comparable elemental concentrations, especially for OC, in the subsize fractions of the 0.7–450 nm colloids (Fig. 2**; Figure S4 and S5**) from the bare fallow and cropped soils suggests that these colloids were less affected by the OM depletion compared to the other much larger soil size fractions, i.e., small SMA. A similar observation was also reported by Jiang et al. (2015), who studied the same sites and found that the 10-years different land management (bare fallow vs cropped) has no pronounced impact on the chemical composition of fine WDCs (<225 nm). For explanation, it should be considered that (i) OM is generally better stabilized in the finer fractions where the presence of high shares of clay minerals promotes the formation of OM-mineral associations optimizing its preservation (Christensen, 2001; Kleber et al., 2015; von Lützow et al., 2007), and that (ii) during the 14 years of bare fallow, OM might be transferred from the coarse to the finest size fraction due to physical breakdown and microbial processing. Chassé et al. (2021) observed that a notable transfer of OM from coarse > 2 μm fractions into the clay fractions of silty loam Luvisols occurred in the first 10 years of bare fallow.

After wet-dry cycles, for both the cropped and bare fallow samples, low concentrations of all the detected elements in the 0.7–450 nm colloids being remained in aggregate suspensions implied that these fine particles were highly involved in aggregation. Intriguingly, a large proportion (~30–40%) of the 0.7–450 nm colloidal OC was present in the first size fraction (0.7–55 nm, **Figure S7 and S8**), being much higher than their counterparts in the added 0.7–450 nm colloids (~3–7%, **Figure 2 and S4**) and in the 0.7–450 nm colloids originally existing in the small SMA (~13%, **Figure S5**). One possible explanation could be that the 0.7–55 nm OC-enriched nanoparticles were less involved in the aggregation process, being remained in the suspensions after wet-dry cycles. Meanwhile, wet-dry cycles could also lead to the release of nanoparticulate and/or colloidal OC in this size range. For instance, release of soluble C after multiple wet-dry cycles was observed in grassland soils (Xiang et al., 2008). Likewise, Gu et al. (2018) reported that drying and rewetting cycles stimulated the release of colloidal P from riparian soils, which was accompanied by the leaching of colloidal OC (5 kDa − 450 nm). Within which, fine nanoparticle OC (5–30 kDa) accounted for >50% of the released colloidal OC. However, Klitzke and Lang (2007) argued that the influence of drying on the dispersibility of colloids in rewetting is likely to depend on their composition, as the authors observed that mainly organic colloids were mobilized by soil drying in a C-rich matrix, whereas (organo)-mineral colloids are immobilized in a more mineral matrix. Note, the dynamic of colloids under wet-dry cycles i.e., incorporation in soil aggregation and/or release of colloids, and its relation to the colloidal properties such as size and chemical composition warrant further investigation.

4.2. Colloidal control of soil aggregate formation in wet-dry cycles

Before wet-dry cycles, for both the cropped and bare fallow soils, soil colloids and small SMA were well dispersed in suspensions without noticeable aggregation (Fig. 3), which could be attributed to the electrostatic repulsion between these particles. Soil compounds like clay minerals and organic matter are commonly negatively charged, making zeta potential values of small SMA negative. For WDCs of soils from the same sites, negative surface charging was reported as well (Jiang et al., 2014). In these soils, at circumneutral pH, the effect of Fe (hydr)oxides with a positive point of zero charge on the bulk surface charge of colloids appears minor.

After wet-dry cycles, an increase in the abundance of the 10–40 μm SMA and formation of aggregates >40 μm, at the expanse of the colloids and 1–10 μm SMA, were observed in all the treatments for both the bare fallow and cropped soils, although the size distribution of aggregates varied among the treatments (Fig. 3**, Table S1**). In general, drying is known to promote aggregation since capillary forces could overcome electrostatically repulsive forces between particles driving them together (Horn and Peth, 2009; Majdalani et al., 2008; Mitchell and Soga, 2005). However, in general the resulting aggregates, especially those formed from large size particles, tend to be unstable when being subjected to rewetting. This is mainly due to (1) the low cohesion between particles (Paradiś et al., 2017; Seiphoori et al., 2020) and (2) the pressure caused by entrapped air inside the pores of the aggregates, which is more prominent when aggregates are submitted into a fast rewetting by sudden immersion than a slow rewetting (i.e., capillary wetting) (Kaiser et al., 2015; Le Bissonnais, 1996). Accordingly, the response of aggregates to wet-dry cycles is likely to vary with the rewetting rate as well as their wettability as observed in many previous studies (e.g., Denef et al., 2002; Wagner et al., 2007).

Yet, in the present study, the 1–40 μm SMA and >40 μm aggregates that formed in wet-dry cycles remained integrated when resuspending in deionized water via a fast rewetting (Fig. 3). The stability of these aggregates against rewetting could be attributed to an enhanced adhesion between particles due to participation of the small particles (i.e., <450 nm colloids) in aggregation of larger particles (i.e., 1–10 μm small SMA) in combination with strengthened near-field interactions between particles due to drying. During drying colloids can be brought to small SMA by the air–water interface and attached to their surfaces by van der Waals forces after complete drying (Paradiś et al., 2017; Wan and Wilson, 1994). Their accumulation on the surface of small SMA provided numerous new potential contact points which were likely to support the formation of aggregates in a close packing in next wet-dry cycles. Moreover, according to previous studies, when soils are subjected to drying, small particles can also be concentrated in the water meniscus of large particles and arranged at their contact areas by capillary forces (Denef et al., 2002; Horn and Dexter, 1989; Majdalani et al., 2008). After complete drying, small particles can turn into solid bridges in the interparticle space, thereby increasing contact points between large particles and reinforcing the interparticle bonds (Seiphoori et al., 2020). As a result, the cohesion force of formed aggregates is enhanced and

strongly dependent on the sum of the van der Waals bonds within the solid bridges of small particles (Seiphoori et al., 2020).

Seiphoori et al. (2020) highlighted the role of <5 μm particles as solid bridges in the formation of stable aggregates. These authors observed that aggregates generated from drying of suspensions of 5–100 μm illite particles readily disintegrated in response to rewetting, whereas aggregates resulting from drying of 0.1–100 μm illite suspensions were stable against rewetting. Yet, compared to these aggregates formed by pure clay minerals, whose stability solely accounted on solid bridges, OC in colloids and small SMA as well as in the <0.7 nm fraction could also contribute to the stability of the formed aggregates. The interparticle cohesion within aggregates was presumably strengthened by the accumulation of colloidal OC and dissolved organic matter in the <0.7 nm fraction at contact points. Albalasmeh and Ghezzehei (2014) found that the water stability of sand aggregates increased with the amount of dissolved/suspended organic matter that was transferred and deposited at the particle contacts during the drying process. Similarly, Park et al. (2007) showed that transport of dissolved organic matter towards the interiors of aggregates subjected to multiple wetting–drying cycles resulted in significant stabilization. Furthermore, the existence of OM was likely to increase the hydrophobicity of the aggregates when subjected to drying (Kaiser et al., 2015). This could decrease the flow rate of infiltrated water (Hallett et al., 2001; Zaher et al., 2005), leading to a reduced effect of slaking on aggregates in the course of rewetting.

Intriguingly, the high abundance of the <1 μm colloids (Fig. 4**b**), especially that of the <450 nm colloids (Fig. 4**a**), in small SMA suspensions seemed to preferentially support the formation of the 1–40 μm SMA, indicating a controlling effect of the colloidal contents on the size distribution of formed aggregates. A possible explanation is that, with the participation of colloids in aggregation, the 1–40 μm SMA were probably a more energetically stable form than larger size ones under the current experiment conditions. It has been proposed that, with repeated wet-dry cycles, the smaller soil particles, such as colloids and clay particles, will be arranged in a way of the lowest free energy, which increase the strength of aggregates (Horn and Dexter, 1989; Horn and Peth, 2009). As mentioned previously, attachment of colloids to small SMA surfaces can provide numerous potential contact points, presumably supporting formation of aggregates in a close packing (i.e., 1–40 μm SMA). In the next wet-dry cycles, these contact points between small SMA could be further strengthened by colloids in water meniscus during the drying. Instead, the formation of the >40 μm large SMA and macroaggregates appeared to be a preferred form in the absence of colloids (Fig. 3k and 3 l). As suggested by Seiphoori et al, (2020), <5 μm particles were crucial to the formation of stable aggregates as serving solid bridges at particle contacts. Therefore, in absence of <1 μm colloids, although small SMA were likely to be bridged by the remaining small particles (i.e., 1–5 μm), contacts points between them were assumed to largely decrease, leading to a preferential formation of >40 μm soil micro- and macroaggregates. However, these mechanisms warrant further investigations.

Besides the particle size, the composition of soil particles, such as small SMA and colloids, is another factor that is considered to influence aggregation and sizes of resulting aggregates. For instance, Fe (hydr) oxides can serve as cementing agents in the formation of aggregates and cause contraction of the porous structure of aggregates, thereby resulting in a more compact structure of aggregates (Jiang et al., 2014; Krause et al., 2020). When Fe (hydr)oxides were removed from colloids and small SMA, Krause et al. (2020) observed that the size distribution of formed aggregates in wet-dry cycles shifted into larger size ranges compared to those aggregates that formed with the presence of Fe (hydr) oxides. This was due to the formation of larger and probably less stable structures between OC and clay particles (Jiang et al., 2014; Krause et al., 2020). In addition, removal of OC from colloids and small SMA impeded their aggregation to the large size aggregates in wet-dry cycles (Krause et al., 2020). However, in the present work, it seems that the composition of the small SMA, which is mainly associated with the presence of pedogenic minerals and SOM, is less important to aggregation under the studied conditions, in contrast to our second hypothesis. Apart from the significant differences in concentrations of C and Fe ($P < 0.05$, Table 2) of small SMA between two soils, the quality of OC and Fe oxides could also be different. A recent study on the same soils reported that compared to the bare fallow soil, the occluded small SMA as well as the bulk soil from the cropped soil contained more poorly crystalline Fe (oxy)hydroxides (Siebers et al., 2024). Moreover, the occluded small SMA from the cropped soil harbored more younger OC than those from the bare fallow one as indicated by the ^{14}C content. These differences in the quality of Fe and OC between two soils were also likely to occur in the free small SMA used in this study. Yet, these differences in the quality and quantity of Fe and OC in small SMA did not lead to significant differences in the size distribution of the resulting aggregates between theses soils ($P > 0.05$, **Table S1**).

Furthermore, all the components in colloids seem to contribute equally to the aggregate formation, as in relative to the deionized water treatments (without added colloids), the enhanced abundance of the 1–40 μm aggregates after wet-dry cycles in other treatments was positively correlated with the concentration of all the measured elements in the added 0.7–450 nm colloids ($r = 0.53–0.55$, $p < 0.01$, Table 3). As discussed above, the OC, Si, Al, Fe, Ca, and Mg in the added 0.7–450 nm colloids were likely located in associations of different soil compounds. In such associations, the individual effect of specific surfaces of the different aggregate forming materials on particle–particle interactions might be altered due to the interplay among them. For instance, positive surface charges of Fe (hydr)oxides particles can be masked if OM and/or clay minerals are attached to their external surfaces (Dultz et al., 2019; Guhra et al., 2019). As a result, it is likely that electrostatic attraction is not one of the decisive processes responsible for aggregation under wet-dry cycles. More important seems to be the presence of fine particles like colloids for the formation of solid bridges between the larger particles, here small SMA. Seiphoori et al. (2020) showed that the interparticle cohesive force of stable aggregates resulting from drying originates from the sum of the van der Waals bonds within the solid bridges of small particles.

However, the aggregation of colloids and small SMA could be affected by the elements in the <0.7 nm fraction of suspensions, within which high concentrations of Ca ($p < 0.01$), along with those of Mg, Si, Al, and OC ($p < 0.05$) contributed to the high abundances of the 1–40 μm aggregates after wet-dry cycles (Table 3). In the drying process, concentrations of polyvalent cations (e.g., Ca^{2+}) and OC increased, which might favor their bridging with negatively charged surfaces of colloids and small SMA (Bronick and Lal, 2005; Regelink et al., 2015). In addition, increased concentrations of polyvalent cations could also induce the coagulation of colloidal- (<1 μm) and clay-sized (<2 μm) particles (Majzik and Tombácz, 2007), generating aggregates in small size ranges. As soil continued to dry, increasing concentrations of dissolved salts could also lead to their surface precipitation (He and Chu, 2017; Mitchell and Soga, 2005). The precipitated salts at contact points between particles can forge strong particle–particle bonds (Holthusen et al., 2012; Mitchell and Soga, 2005), facilitating aggregate formation. Cations such as Ca^{2+} have been suggested to stimulate the precipitation of compounds that act as cementing agents for soil aggregates (Bronick and Lal, 2005).

5. Conclusion

Colloids have been suggested to play an important role in the formation of soil structure. While their contribution to the development of composite building units, i.e., organo-mineral and mineral–mineral associations of aggregates was extensively studied, up to now, little is known on how the participation of colloids in soil aggregation regulates aggregate build-up. Our findings suggested that the colloidal content controls the aggregation of small SMA in wet-dry cycles thereby regulating the size distribution of the resulting aggregates. For the studied

soils, a high abundance of <450 nm colloids could induce attachment of colloids to small SMA surfaces which provided numerous potential contact points favoring the formation of aggregates in a close packing, i.e., 1–40 μm SMA. In the following wet-dry cycles, these contact points between small SMA might be further strengthened by colloids in water meniscus during drying. In contrast, in absence of <1 μm colloids, contacts points between small SMA were assumed to largely decrease, although they were likely to be bridged by the remaining small particles (i.e., 1–5 μm), leading to a preferential formation of >40 μm soil micro- and macroaggregates. Furthermore, the independence of this colloidal controlling effect from the composition of small SMA and colloids implied that, under the studied conditions, the size of particles was more decisive than their compositions for the formation and the size distribution of aggregates resulting from wet-dry cycles. Overall, these results underline the importance of soil particle size in aggregate formation and an indispensable role of soil colloids in the formation of small-sized SMA and therefore in the development of the aggregate hierarchy.

CRediT authorship contribution statement

Ni Tang: Conceptualization, Methodology, Investigation, Visualization, Data curation, Validation, Formal analysis, Writing – original draft, Writing – review & editing. **Stefan Dultz:** Resources, Writing – review & editing. **Daniel Gerth:** Investigation, Formal analysis. **Erwin Klumpp:** Conceptualization, Writing – review & editing, Funding acquisition, Supervision, Resources, Project administration.

Declaration of competing interest

The authors declare that they have no known competing financial interests or personal relationships that could have appeared to influence the work reported in this paper.

Data availability

All relevant data are included in the Supplementary materials

Acknowledgements

This work is associated with the MAD Soil project (MAD Soil - Microaggregates: Formation and turnover of the structural building blocks of soils), which is funded by the DFG (Deutsche Forschungsgemeinschaft, Research Unit 2179). Ni Tang appreciates the China Scholarship Council (No. 201806190224) for supporting her studies at Forschungszentrum Jülich and RWTH Aachen University. Additionally, we would like to thank *Liming Wang* for assisting with size fractionation.

Appendix A. Supplementary data

Supplementary data to this article can be found online at https://doi.org/10.1016/j.geoderma.2024.116830.

References

Albalasmeh, A.A., Ghezzehei, T.A., 2014. Interplay between soil drying and root exudation in rhizosheath development. Plant and Soil 374 (1), 739–751. https://doi.org/10.1007/s11104-013-1910-y.

Amelung, W., Tang, N., Siebers, N., Aehnelt, M., Eusterhues, K., Felde, V.J.M.N.L., Guggenberger, G., Kaiser, K., Kögel-Knabner, I., Klumpp, E., Knief, C., Kruse, J., Lehndorff, E., Mikutta, R., Peth, S., Ray, N., Prechtel, A., Ritschel, T., Schweizer, S. A., Woche, S.K., Wu, B., Totsche, K.U., 2024. Architecture of soil microaggregates: Advanced methodologies to explore properties and functions. J. Plant Nutrit. Soil Sci. 187 (1), 17–50. https://doi.org/10.1002/jpln.202300149.

Asano, M., Wagai, R., 2014. Evidence of aggregate hierarchy at micro- to submicron scales in an allophanic Andisol. Geoderma 216, 62–74. https://doi.org/10.1016/j.geoderma.2013.10.005.

Asano, M., Wagai, R., Yamaguchi, N., Takeichi, Y., Maeda, M., Suga, H., Takahashi, Y., 2018. In search of a binding agent: nano-scale evidence of preferential carbon associations with poorly-crystalline mineral phases in physically-stable, clay-sized aggregates. Soil Syst. 2 (2), 32. https://doi.org/10.3390/soilsystems2020032.

Bai, T., Wang, P., Hall, S.J., Wang, F., Ye, C., Li, Z., Li, S., Zhou, L., Qiu, Y., Guo, J., Guo, H., Wang, Y., Hu, S., 2020. Interactive global change factors mitigate soil aggregation and carbon change in a semi-arid grassland. Glob. Change Biol. 26 (9), 5320–5332. https://doi.org/10.1111/gcb.15220.

Bieganowski, A., Ryżak, M., Sochan, A., Barna, G., Hernádi, H., Beczek, M., Polakowski, C., Makó, A., 2018. Chapter Five - laser diffractometry in the measurements of soil and sediment particle size distribution. In: Sparks, D.L. (Ed.), Adv. Agron. Academic Press, pp. 215–279. https://doi.org/10.1016/bs.agron.2018.04.003.

Blanco-Canqui, H., Lal, R., 2004. Mechanisms of Carbon Sequestration in Soil Aggregates. Crit. Rev. Plant Sci. 23 (6), 481–504. https://doi.org/10.1080/07352680490886842.

Bronick, C.J., Lal, R., 2005. Soil structure and management: a review. Geoderma 124 (1), 3–22. https://doi.org/10.1016/j.geoderma.2004.03.005.

Chassé, M., Lutfalla, S., Cécillon, L., Baudin, F., Abiven, S., Chenu, C., Barré, P., 2021. Long-term bare-fallow soil fractions reveal thermo-chemical properties controlling soil organic carbon dynamics. Biogeosciences 18 (5), 1703–1718. https://doi.org/10.5194/bg-18-1703-2021.

Christensen, B.T., 2001. Physical fractionation of soil and structural and functional complexity in organic matter turnover. Eur. J. Soil Sci. 52 (3), 345–353. https://doi.org/10.1046/j.1365-2389.2001.00417.x.

Denef, K., Six, J., Merckx, R., Paustian, K., 2002. Short-term effects of biological and physical forces on aggregate formation in soils with different clay mineralogy. Plant Soil 246 (2), 185–200. https://doi.org/10.1023/A:1020668013524.

Dultz, S., Woche, S.K., Mikutta, R., Schrapel, M., Guggenberger, G., 2019. Size and charge constraints in microaggregation: Model experiments with mineral particle size fractions. Applied Clay Science 170, 29–40. https://doi.org/10.1016/j.clay.2019.01.002.

Gonzalez, J.M., Laird, D.A., 2003. Carbon Sequestration in Clay Mineral Fractions from 14C-Labeled Plant Residues. Soil Science Society of America Journal 67 (6), 1715–1720. https://doi.org/10.2136/sssaj2003.1715.

Gu, S., Gruau, G., Malique, F., Dupas, R., Petitjean, P., Gascuel-Odoux, C., 2018. Drying/rewetting cycles stimulate release of colloidal-bound phosphorus in riparian soils. Geoderma 321, 32–41. https://doi.org/10.1016/j.geoderma.2018.01.015.

Guhra, T., Ritschel, T., Totsche, K.U., 2019. Formation of mineral–mineral and organo–mineral composite building units from microaggregate-forming materials including microbially produced extracellular polymeric substances. European Journal of Soil Science 70 (3), 604–615. https://doi.org/10.1111/ejss.12774.

Guhra, T., Stolze, K., Totsche, K.U., 2022. Pathways of biogenically excreted organic matter into soil aggregates. Soil Biol. Biochem. 164, 108483 https://doi.org/10.1016/j.soilbio.2021.108483.

Hallett, P.D., Baumgartl, T., Young, I.M., 2001. Subcritical Water Repellency of Aggregates from a Range of Soil Management Practices. Soil Science Society of America Journal 65 (1), 184–190. https://doi.org/10.2136/sssaj2001.651184x.

He, J., Chu, J., 2017. Cementation of sand due to salt precipitation in drying process. Mar. Georesources Geotechnol. 35 (3), 441–445. https://doi.org/10.1080/1064119X.2016.1168498.

Hochman, D., Dor, M., Mishael, Y., 2021. Diverse effects of wetting and drying cycles on soil aggregation: Implications on pesticide leaching. Chemosphere 263, 127910. https://doi.org/10.1016/j.chemosphere.2020.127910.

Holthusen, D., Peth, S., Horn, R., Kühn, T., 2012. Flow and deformation behavior at the microscale of soils from several long-term potassium fertilization trials in Germany. J. Plant Nutr. Soil Sci. 175 (4), 535–547. https://doi.org/10.1002/jpln.201100073.

Horn, R., Dexter, A.R., 1989. Dynamics of soil aggregation in an irrigated desert loess. Soil Tillage Res. 13 (3), 253–266. https://doi.org/10.1016/0167-1987(89)90002-0.

Horn, R., Peth, S., 2009. Soil structure formation and management effects on gas emission. Biologia 64 (3), 449–453. https://doi.org/10.2478/s11756-009-0089-4.

Horn, R., Taubner, H., Wuttke, M., Baumgartl, T., 1994. Soil physical properties related to soil structure. Soil Tillage Res. 30 (2), 187–216. https://doi.org/10.1016/0167-1987(94)90005-1.

IUSS Working Group WRB, 2007. World Reference Base for Soil Resources 2006, first update 2007. World Soil Resources Reports No. 103. FAO, Rome.

Jiang, X., Bol, R., Nischwitz, V., Siebers, N., Willbold, S., Vereecken, H., Amelung, W., Klumpp, E., 2015. Phosphorus Containing Water Dispersible Nanoparticles in Arable Soil. J. Environ. Qual. 44 (6), 1772–1781. https://doi.org/10.2134/jeq2015.02.0085.

Jiang, C., Séquaris, J.-M., Wacha, A., Bóta, A., Vereecken, H., Klumpp, E., 2014. Effect of metal oxide on surface area and pore size of water-dispersible colloids from three German silt loam topsoils. Geoderma 235–236, 260–270. https://doi.org/10.1016/j.geoderma.2014.07.017.

Kaiser, M., Kleber, M., Berhe, A.A., 2015. How air-drying and rewetting modify soil organic matter characteristics: An assessment to improve data interpretation and inference. Soil Biol. Biochem. 80, 324–340. https://doi.org/10.1016/j.soilbio.2014.10.018.

Kleber, M., Eusterhues, K., Keiluweit, M., Mikutta, C., Mikutta, R., Nico, P.S., 2015. Chapter one - mineral-organic associations: formation, properties, and relevance in soil environments. In: Sparks, D.L. (Ed.), Adv. Agron. Academic Press, pp. 1–140. https://doi.org/10.1016/bs.agron.2014.10.005.

Klitzke, S., Lang, F., 2007. Hydrophobicity of soil colloids and heavy metal mobilization. J. Environ. Quality 36 (4), 1187–1193. https://doi.org/10.2134/jeq2006.0427.

Krause, L., Rodionov, A., Schweizer, S.A., Siebers, N., Lehndorff, E., Klumpp, E., Amelung, W., 2018. Microaggregate stability and storage of organic carbon is affected by clay content in arable Luvisols. Soil Tillage Res. 182, 123–129. https://doi.org/10.1016/j.still.2018.05.003.

Krause, L., Klumpp, E., Nofz, I., Missong, A., Amelung, W., Siebers, N., 2020. Colloidal iron and organic carbon control soil aggregate formation and stability in arable Luvisols. Geoderma 374, 114421. https://doi.org/10.1016/j.geoderma.2020.114421.

Laird, D.A., Martens, D.A., Kingery, W.L., 2001. Nature of Clay-Humic Complexes in an Agricultural Soil. Soil Sci. Soc. Am. J. 65 (5), 1413–1418. https://doi.org/10.2136/sssaj2001.6551413x.

Le Bissonnais, Y., 1996. Aggregate stability and assessment of soil crustability and erodibility: I. Theory and methodology. Eur. J. Soil Sci. 47 (4), 425–437. https://doi.org/10.1111/j.1365-2389.1996.tb01843.x.

Lehmann, J., Kinyangi, J., Solomon, D., 2007. Organic matter stabilization in soil microaggregates: implications from spatial heterogeneity of organic carbon contents and carbon forms. Biogeochemistry 85 (1), 45–57. https://doi.org/10.1007/s10533-007-9105-3.

Li, F., Zhang, Q., Klumpp, E., Bol, R., Nischwitz, V., Ge, Z., Liang, X., 2021. Organic carbon linkage with soil colloidal phosphorus at regional and field scales: insights from size fractionation of fine particles. Environ. Sci. Technol. 55 (9), 5815–5825. https://doi.org/10.1021/acs.est.0c07709.

Lützow, M.V., Kögel-Knabner, I., Ekschmitt, K., Matzner, E., Guggenberger, G., Marschner, B., Flessa, H., 2006. Stabilization of organic matter in temperate soils: mechanisms and their relevance under different soil conditions – a review. Eur. J. Soil Sci. 57 (4), 426–445. https://doi.org/10.1111/j.1365-2389.2006.00809.x.

Majdalani, S., Michel, E., Di-Pietro, L., Angulo-Jaramillo, R., 2008. Effects of wetting and drying cycles on in situ soil particle mobilization. Eur. J. Soil Sci. 59 (2), 147–155. https://doi.org/10.1111/j.1365-2389.2007.00964.x.

Majzik, A., Tombácz, E., 2007. Interaction between humic acid and montmorillonite in the presence of calcium ions II. Colloidal interactions: Charge state, dispersing and/or aggregation of particles in suspension. Org. Geochem. 38 (8), 1330–1340. https://doi.org/10.1016/j.orggeochem.2007.04.002.

Meyer, N., Bornemann, L., Welp, G., Schiedung, H., Herbst, M., Amelung, W., 2017. Carbon saturation drives spatial patterns of soil organic matter losses under long-term bare fallow. Geoderma 306, 89–98. https://doi.org/10.1016/j.geoderma.2017.07.004.

Mikutta, R., Schaumann, G.E., Gildemeister, D., Bonneville, S., Kramer, M.G., Chorover, J., Chadwick, O.A., Guggenberger, G., 2009. Biogeochemistry of mineral–organic associations across a long-term mineralogical soil gradient (0.3–4100kyr), Hawaiian Islands. Geochim. Cosmochim. Acta. 73 (7), 2034–2060. https://doi.org/10.1016/j.gca.2008.12.028.

Missong, A., Bol, R., Nischwitz, V., Krüger, J., Lang, F., Siemens, J., Klumpp, E., 2018. Phosphorus in water dispersible-colloids of forest soil profiles. Plant Soil 427 (1), 71–86. https://doi.org/10.1007/s11104-017-3430-7.

Mitchell, J.K., Soga, K., 2005. Fundamentals of soil behavior, third ed. John Wiley & Sons New York.

Nam, K., Kim, J.Y., Oh, D.I., 2003. Effect of soil aggregation on the biodegradation of phenanthrene aged in soil. Environ. Pollut. 121 (1), 147–151. https://doi.org/10.1016/S0269-7491(02)00181-1.

Nguyen, M.N., Dultz, S., Meharg, A., Pham, Q.V., Hoang, A.N., Dam, T.T.N., Nguyen, V. T., Nguyen, K.M., Nguyen, H.X., Nguyen, N.T., 2019. Phytolith content in Vietnamese paddy soils in relation to soil properties. Geoderma 333, 200–213. https://doi.org/10.1016/j.geoderma.2018.07.027.

Nischwitz, V., Gottselig, N., Missong, A., Meyn, T., Klumpp, E., 2016. Field flow fractionation online with ICP-MS as novel approach for the quantification of fine particulate carbon in stream water samples and soil extracts. J. Anal. At. Spectrom 31 (9), 1858–1868. https://doi.org/10.1039/C6JA00027D.

Oades, J., Waters, A., 1991. Aggregate hierarchy in soils. Soil Res. 29 (6), 815–828. https://doi.org/10.1071/SR9910815.

Paradelo, R., van Oort, F., Barré, P., Billiou, D., Chenu, C., 2016. Soil organic matter stabilization at the pluri-decadal scale: Insight from bare fallow soils with contrasting physicochemical properties and macrostructures. Geoderma 275, 48–54. https://doi.org/10.1016/j.geoderma.2016.04.009.

Paradiś, A., Brueck, C., Meisenheimer, D., Wanzek, T., Dragila, M.I., 2017. Sandy soil microaggregates: rethinking our understanding of hydraulic function. vzj2017.2005.0090 Vadose Zone J. 16 (9). https://doi.org/10.2136/vzj2017.05.0090.

Park, E.-J., Sul, W.J., Smucker, A.J.M., 2007. Glucose additions to aggregates subjected to drying/wetting cycles promote carbon sequestration and aggregate stability. Soil Biol. Biochem. 39 (11), 2758–2768. https://doi.org/10.1016/j.soilbio.2007.06.007.

Rabot, E., Wiesmeier, M., Schlüter, S., Vogel, H.J., 2018. Soil structure as an indicator of soil functions: A review. Geoderma 314, 122–137. https://doi.org/10.1016/j.geoderma.2017.11.009.

Regelink, I.C., Stoof, C.R., Rousseva, S., Weng, L., Lair, G.J., Kram, P., Nikolaidis, N.P., Kercheva, M., Banwart, S., Comans, R.N.J., 2015. Linkages between aggregate formation, porosity and soil chemical properties. Geoderma 247–248, 24–37. https://doi.org/10.1016/j.geoderma.2015.01.022.

Rowley, M.C., Grand, S., Verrecchia, E.P., 2018. Calcium-mediated stabilisation of soil organic carbon. Biogeochemistry 137 (1–2), 27–49. https://doi.org/10.1007/s10533-017-0410-1.

Schweizer, S.A., Aehnelt, M., Bucka, F., Totsche, K.U., Kögel-Knabner, I., 2024. Impact of bare fallow management on soil carbon storage and aggregates across a rock fragment gradient. J. Plant Nutrit. Soil Sci. 187 (1), 118–129. https://doi.org/10.1002/jpln.202300156.

Seiphoori, A., Ma, X.-G., Arratia, P.E., Jerolmack, D.J., 2020. Formation of stable aggregates by fluid-assembled solid bridges. Proc. Natl. Acad. Sci. u.s.a. 117 (7), 3375–3381. https://doi.org/10.1073/pnas.1913855117.

Seiphoori, A., Zamanian, M., 2022. Improving mechanical behaviour of collapsible soils by grouting clay nanoparticles. Eng. Geol. 298, 106538 https://doi.org/10.1016/j.enggeo.2022.106538.

Siebers, N., Voggenreiter, E., Joshi, P., Rethemeyer, J., Wang, L., 2024. Synergistic relationships between the age of soil organic matter, Fe speciation, and aggregate stability in an arable Luvisol. J. Plant Nutrit. Soil Sci. 187 (1), 77–88. https://doi.org/10.1002/jpln.202300020.

Six, J., Elliott, E.T., Paustian, K., 2000. Soil macroaggregate turnover and microaggregate formation: a mechanism for C sequestration under no-tillage agriculture. Soil Biol. Biochem. 32 (14), 2099–2103. https://doi.org/10.1016/S0038-0717(00)00179-6.

Tang, N., Siebers, N., Leinweber, P., Eckhardt, K.-U., Dultz, S., Nischwitz, V., Klumpp, E., 2022. Implications of Free and Occluded Fine Colloids for Organic Matter Preservation in Arable Soils. Environ. Sci. Technol. 56 (19), 14133–14145. https://doi.org/10.1021/acs.est.2c01973.

Totsche, K.U., Amelung, W., Gerzabek, M.H., Guggenberger, G., Klumpp, E., Knief, C., Lehndorff, E., Mikutta, R., Peth, S., Prechtel, A., Ray, N., Kögel-Knabner, I., 2018. Microaggregates in soils. J. Plant. Nutr. Soil Sci. 181 (1), 104–136. https://doi.org/10.1002/jpln.201600451.

Verchot, L.V., Dutaur, L., Shepherd, K.D., Albrecht, A., 2011. Organic matter stabilization in soil aggregates: Understanding the biogeochemical mechanisms that determine the fate of carbon inputs in soils. Geoderma 161 (3), 182–193. https://doi.org/10.1016/j.geoderma.2010.12.017.

Virto, I., Barré, P., Chenu, C., 2008. Microaggregation and organic matter storage at the silt-size scale. Geoderma 146 (1), 326–335. https://doi.org/10.1016/j.geoderma.2008.05.021.

von Lützow, M., Kögel-Knabner, I., Ekschmitt, K., Flessa, H., Guggenberger, G., Matzner, E., Marschner, B., 2007. SOM fractionation methods: Relevance to functional pools and to stabilization mechanisms. Soil Biol. Biochem. 39 (9), 2183–2207. https://doi.org/10.1016/j.soilbio.2007.03.007.

Wagai, R., Kajiura, M., Asano, M., 2020. Iron and aluminum association with microbially processed organic matter via meso-density aggregate formation across soils: organo-metallic glue hypothesis. Soil 6 (2), 597–627. https://doi.org/10.5194/soil-6-597-2020.

Wagner, S., Cattle, S.R., Scholten, T., 2007. Soil-aggregate formation as influenced by clay content and organic-matter amendment. J. Plant Nutrit. Soil Sci. 170 (1), 173–180. https://doi.org/10.1002/jpln.200521732.

Wan, J., Wilson, J.L., 1994. Visualization of the role of the gas-water interface on the fate and transport of colloids in porous media. Water Resour. Res. 30 (1), 11–23. https://doi.org/10.1029/93WR02403.

Wang, L., Xue, C., Zhang, Y., Li, Z., Liu, C., Pan, X., Chen, F., Liu, Y., 2018. Soil aggregate-associated distribution of DDTs and HCHs in farmland and bareland soils in the Danjiangkou Reservoir Area of China. Environ. Pollut. 243, 734–742. https://doi.org/10.1016/j.envpol.2018.09.019.

Xiang, S.-R., Doyle, A., Holden, P.A., Schimel, J.P., 2008. Drying and rewetting effects on C and N mineralization and microbial activity in surface and subsurface California grassland soils. Soil Biol. Biochem. 40 (9), 2281–2289. https://doi.org/10.1016/j.soilbio.2008.05.004.

Zaher, H., Caron, J., Ouaki, B., 2005. Modeling aggregate internal pressure evolution following immersion to quantify mechanisms of structural stability. Soil Sci. Soc. Am. J. 69 (1), 1–12. https://doi.org/10.2136/sssaj2005.0001.

Zech, S., Schweizer, S.A., Bucka, F.B., Ray, N., Kögel-Knabner, I., Prechtel, A., 2022. Explicit spatial modeling at the pore scale unravels the interplay of soil organic carbon storage and structure dynamics. Glob. Change Biol. 28 (15), 4589–4604. https://doi.org/10.1111/gcb.16230.

Zhang, Q., Bol, R., Amelung, W., Missong, A., Siemens, J., Mulder, I., Willbold, S., Müller, C., Westphal Muniz, A., Klumpp, E., 2021. Water dispersible colloids and related nutrient availability in Amazonian Terra Preta soils. Geoderma 397, 115103. https://doi.org/10.1016/j.geoderma.2021.115103.

Zhang, G.S., Liu, Y.F., 2018. The distribution of microplastics in soil aggregate fractions in southwestern China. Sci. Total Environ. 642, 12–20. https://doi.org/10.1016/j.scitotenv.2018.06.004.